Electronic Supplementary Information

Genetics of Superionic Conductivity in Lithium Lanthanum Titanates

E. E. Jay[a], M. J. D. Rushton[a], A. Chroneos[b], R.W. Grimes[a] and J. A. Kilner[a,*]

[a]*Department of Materials, Imperial College, London, SW7 2AZ, United Kingdom*

[b]*Faculty of Engineering and Computing, Coventry University, 3 Gulson Street, Coventry CV1 2JH, United Kingdom*

LLTO systems with low lithium contents ($x \leq 0.08$) have predominately been found to adopt an orthorhombic structure and at lithium contents above this, a tetragonal structure forms[20], space group P4/mmm, figure 1a. The unit cell of LLTO is made from TiO_6 octahedra and the A-cation cages are formed by 12 oxygen ions belonging to octahedra[21,22], see figure 1a. It is difficult to describe the defect nomenclature based on the $La_{2/3}TiO_3$ lattice and thereby to ensure a consistent notation and set of effective charges. Nevertheless, to describe point defects using Kröger-Vink notation[23] the $A^{2+}B^{4+}O_3$ stoichiometry of the parent structure will be used. The La^{3+} ions randomly populate the A-sites ($La_A^{\bullet}$), however, there is a small degree of ordering forming rich and poor $La_A^{\bullet}$ layers along the *c*-axis. Lithium ions and A site vacancies also occupy the A-sites, leaving a network of Li_A' and V_A'' available for lithium ion migration[7]. In the notation chosen for this representation the neutrality condition becomes;

$$2[V_A''] + [Li_A'] = [La_A^{\bullet}] \quad (2)$$

The effect of the $La_A^{\bullet}$ layering is of particular importance to the migration and movement of Li_A' ions between the layers[24]. The degree of ordering of cations and vacancies on the A-sites in the layers strongly influences the crystal structure and Li ion conductivity[17] and it is important to define the stoichiometry, degree of ordering and crystal structure when comparing conductivity results. The crystal is described as having rich and poor La layers[17] and an order parameter describing the degree of order is defined as $S = \frac{R_{(La-rich)} - R_{(dis)}}{1 - R_{(dis)}}$

Where $R_{(La-rich)}$ and $R_{(dis)}$ are the occupancies of the A-sites by La^{3+} ions in a structure with ordered La-rich layers and a disordered structure respectively. For structures where *S*=0, the ions are completely disordered and the diffusion is isotropic. However, when *S*=1 the La rich

planes are fully occupied and the diffusion is restricted to the La poor planes perpendicular the c-axis. The layering effect is an important structural feature since the migration energy barrier for Li^+ ions will depend upon the individual local environment of each of the A-sites along the percolating Li_A' and V_A'' network. As such, there will be no single activation energy for diffusion to describe the transport of Li^+ ions. Therefore, the distribution of the Li_A' and V_A'' in and between the layers is investigated in this work.

In the following section the methodological aspects of the current work are provided. The simulations described within the paper were performed using a simulation box based on a 14×14×14 $La_{⅔}TiO_3$ super-cell into which V_A'' and Li_A' defects were introduced to give a composition of $La_{⅔-x}Li_{3x}TiO_{3-x}$ with x=0.115. An initial set of atomic configurations was generated such that these defects were distributed at random across the La sites of the perfect $La_{⅔}TiO_3$ structure. In order to better understand which defect arrangements gave high Li ion mobility a genetic algorithm (GA) was employed to search for high diffusivity atomic configurations (the details of which are given below).

Systems with *S* parameter values between 0.0 and 0.8 were refined using the GA. Following GA optimisation runs, structures with the highest Li diffusivities were equilibrated further using molecular dynamics (MD) within the temperature range 400-1200K before final MD data-collection runs were performed.

The specific details of the genetic algorithm are now given, after which the MD equilibration and data-collection stages of the process are described. The methodology then concludes with a description of the pair-potential model and how it was developed for this work. The potentials are particularly important as they describe the interatomic forces within the MD simulations underpinning the GA and data-collection runs.

Genetic algorithms aim to mimic the processes of Darwinian evolution. An initial set (or population) of possible solutions to a problem are generated, and over a series of iterations, these are combined using methods imitating sexual reproduction, by which child solutions inherit characteristics from the parents from which they were generated.

At the heart of the method is the principle of 'survival of the fittest', through which population members yielding desirable properties (in this case, high ionic conductivity), are preferentially selected when choosing the parents used to produce the next generation of solutions. By favouring population members with favourable attributes, such as high Li

mean squared displacement, these characteristics should become increasingly prevalent within the population whilst deleterious features will die out as the algorithm progresses. Therefore, over a number of iterations progressive refinement of the solutions may occur.

The method by which pairs of atomic structures were chosen as parents of structures for the following iteration of the genetic algorithm is known as selection. Within the present work roulette wheel selection was employed[27]. As its name suggests this method is conceptually similar to the roulette wheel within a casino; a notional wheel is divided into segments, one belonging to each member of the GA's population. A random number is chosen, representing a ball spinning within the wheel. The segment in which this conceptual ball lands, is used to select a parent structure.

At each iteration of the GA, a fitness value was calculated for each structure in the population (here Li ion mean squared displacement was used, see below). In roulette wheel selection each wheel segment is scaled to be proportional to its candidate's fitness value. In this way, the structures are effectively ranked, with those yielding higher Li mean squared displacement have a higher probability of selection (as their larger segments on the wheel provide a larger target for the notional roulette ball). Although structures with smaller MSDs are less likely to be selected, it can still occur, this is important as it helps to ensure that variety is maintained within the population; without this, it is possible the population to effectively become a set of facsimiles of only a small number of structures and for the algorithm to become stuck in a local minimum (the biological equivalent of this would be in-breeding).

The particular characteristics of each population member are encoded as a set of chromosomes and the set of chromosomes that encode for each population member are referred to as the genome. In the context of the current problem, the layered nature of LLTO affords a natural mapping between the crystal structure and the concept of chromosomes: a single chromosome within the GA represented each *ab* layer of the La sub-lattice.

As the simulation box used was a super-cell constructed from 14×14×14 individual unit-cells, the La sub-lattice contained 14 layers and each layer contained 196 sites (including all the La, Li_A' and V_A'' species within the layer). The initial cell, before Li and vacancies were assigned therefore had the following composition $La_{2744}Ti_{2744}O_{8232}$; initial simulation cell lengths of a=b=54.18Å and c=54.46Å were used. This initial configuration meant that within the genetic algorithm, each atomic configuration was described as 14 lists each

containing 196 entries. Each list entry was one of La, Li_A' or V_A'', with the number of each of these species chosen to give the desired composition. Further, the composition of each layer was chosen to give the appropriate disorder parameter (*S*) such that alternating rich and poor layers were described.

A GA population size of 100 configurations was used. The initial population (i.e. the atomic structures representing the first generation), was initialised by randomly assigning V_A'', Li_A' and La across each structure's layer chromosomes to give the desired composition and *S* parameter.

As the aim of the genetic algorithm was to search for arrangements of Li_A' and V_A'' giving rise to high ionic conductivity the fitness criterion used during selection was each structure's Li mean squared displacement (MSD). High MSD values yield high ionic conductivities; as a result those population members whose structural characteristics gave rise to high MSD values were favoured during selection.

At each iteration, Li MSD values were obtained for each structure from MD calculations with a simulated duration of 5ps at a temperature of 1000K. Given the relatively slow convergence typical of genetic algorithms and the significant number of calculations required at each iterations, this relatively high simulation temperature was chosen in order to allow the method to remain computationally tractable; at 1200K significant Li diffusion is observed even over these relatively short simulation times. During the MSD simulations an integration time-step of 4fs was used.

Within the GA successive generations are obtained by selecting pairs of structures (parents) that are combined to form the next population of structures. In combining the two parents the intent is to obtain resultant structures that have characteristics of both parents. Given that parents are preferentially selected on the basis of high Li mobility, assuming the structural characteristics, giving rise to the high mobilities are maintained in the child structure, then properties superior to either parent may be obtained. Through this mechanism, significant increases in Li ion migration were obtained after several iterations of the genetic algorithm (see the main text). In order for this to occur a method for effectively combining two structures was required. In the present work, single-point crossover was adopted[27].

In single-point crossover, each parent structure is effectively bisected at a randomly chosen lattice site, in so-doing two sections are formed: one for sites occurring before the

bisection point and one after (henceforth referred to as A and B). Two children are formed from these by swapping section B between the two parents. Referring to each parent as M and F respectively, this process yields the following child structures: $A_M B_F$ and $A_F B_M$.

In terms of the genome description of the problem, crossover is achieved by selecting one of the fourteen La layers/chromosome and then picking a random bisection point within the 196 item list which encodes that V_A'', Li_A', La_{La} layer within the algorithm. For each generation a crossover rate of 0.9 was used, meaning that 90% of the configurations were the result of cross-over, the remaining 10% were inherited directly from the previous generation.

Whilst each La layer has a set composition, there can be considerable spatial inhomogeneity across a layer. This means that, although it is straightforward to swap entire layers lying before and after the crossover bisection point, swapping the layer portions within the bisected layer creates child layers that are most probably different in composition to its parents. For this reason, the structures resulting from cross-over underwent a compositional correction step: within the bisected layers, V_A'' and Li_A' species were randomly added or removed as necessary to return the layer to its parent's composition. It should be noted that this effectively represents an implicit structural mutation that acts in addition to the explicit mutation methods described next.

Mutation is used within GAs to preserve and increase the variety of the population. In order to avoid the genetic algorithm from getting trapped in shallow local minima, structural mutations were introduced following cross-over. In addition to the implicit mutation that results from the crossover composition correction, two additional mutations were used. The first involved in-layer swaps where heterogeneous pairs of La, V_A'' and Li_A' species were swapped within the same layer. This mutation was applied with a 5% mutation rate meaning that 27 swaps were performed within 5 of the structure's 14 layers. The second mutation involved entire layers of the La sub-lattice being swapped, allowing the algorithm to explore layer ordering effects more effectively. In order to maintain the correct rich-poor layer ordering, rich layers were only swapped with other rich layers, likewise a poor layer could only be swapped with another poor layer.

For each child structure, only one of these two mutation methods was chosen at random and applied to 2% of the structures within each generation's population.

After the GA had been run for 20 generations the ten configurations exhibiting the highest Li MSD values were selected from the final population for further MD equilibration and data collection stages. The results of these runs form the basis of the results presented within the main text. MD simulations were performed at 100K intervals for temperatures in the range 400K to 1200K. Prior to each data collection run, the system was equilibrated for 20 ps in the NPT ensemble using a Nosé-Hoover thermostat and barostat[45-47] to bring the system to temperature and to allow the system volume to relax. This was followed by another 100 ps of dynamics during which atomic positions were sampled every 100 fs. In comparison to the GA MSD runs, these data-collection runs used a shorter time-step of 1fs.

Molecular dynamics allows the trajectories of a set of atoms to be predicted as a function of time by integrating Newton's laws of motion (here MD calculations were performed using the DL_POLY code[42]). Key to the method's success is an accurate description of the forces acting between atoms. Here, a classical Born[43] description of the crystal lattice was used and long range electrostatic interactions were calculated using the Ewald sum[44] and short range interactions were described using effective pair potentials to give the energies between pairs of anions and anion-cation pairs. These were described using the Buckingham form[41], where two ions *i* and *j*, separated by a distance r_{ij} interact with an energy, Φ, given by,

$$\Phi(r_{ij}) = A\exp\left(-\frac{r_{ij}}{\rho}\right) - \frac{C}{r_{ij}^6} \qquad (3)$$

where, A, ρ and C are parameters specific to pairs of interacting species. Initial calculations (see main text) used the potential parameters of Cleave[30]. These potentials were found to reproduce the thermal properties of LLTO with insufficient fidelity. As a result, a new potential model was derived via an empirical multi-compound approach: potential parameters were adjusted, iteratively, to improve the quality of the model's ability to predict experimental property values, namely unit-cell parameters, elastic constants and thermal expansion coefficients. By fitting to several structures at once, the aim was to produce a robust model that could describe a wide range of atomic environments over a large temperature range. For this reason that stannate and zirconate materials, in addition to the more obvious binary oxide lithium, lanthanum and titanate compounds were used within the fitting procedure. Even though they are not directly relevant to LLTO they helped to improve parameters for the La-O, Li-O and O-O interactions.

Initially fitting was performed against the structures of Li_2O, Li_2TiO_3, La_2O_3, Li_2ZrO_3, ZrO_2, SnO_2, $La_2Sn_2O_7$, $La_2Zr_2O_7$ and TiO_2 (rutile) by using static energy minimisation within the GULP code. The database of fitting properties additionally included bulk-moduli for the Li_2O, La_2O_3 and TiO_2 structures. In order to capture temperature dependent effects, MD runs were used to fit against the thermal expansion coefficients of TiO_2, Li_2TiO_3, Li_2ZrO_3, Li_2O and La_2O_3. The potential parameters resulting from this fitting procedure are given in table 1. For both potential models a short-range cut-off of 10Å was used (beyond which short range interactions are considered to be negligible).

Table 1: Buckingham[39] short-range potential parameters produced for this work.

Species	A (eV)	ρ (Å)	C (eVÅ^6)
$O^{-1.4}$ - $O^{-1.4}$	4869.99	0.24019	27.22
$La^{2.1}$ - $O^{-1.4}$	14509.63	0.24381	30.38
$Ti^{2.8}$ - $O^{-1.4}$	689.14	0.31628	0.00
$Li^{0.7}$ - $O^{-1.4}$	876.86	0.24426	0.00

Ionic diffusion is predicted by tracking the mean square displacement (MSD) of ions as a function of time for the temperature range. At time t the MSD of an ion i at a position $r_i(t)$ at time t with respect to its initial position $r_i(0)$ is,

$$\langle r_i^2(t)\rangle = \frac{1}{N}\sum_{i=1}^{N}[r_i(t) - r_i(0)]^2$$

where N is the total number of ions in the system.

The diffusion coefficient, D, is calculated directly from the slopes of MSD in the given temperature range:

$$\langle |r_i(t) - r_i(0)|^2 \rangle = 6\,Dt + B$$

where $|r_i(t) - r_i(0)|$ is the displacement of an oxygen ion from its initial position and B is an atomic displacement parameter attributed to thermal vibrations.

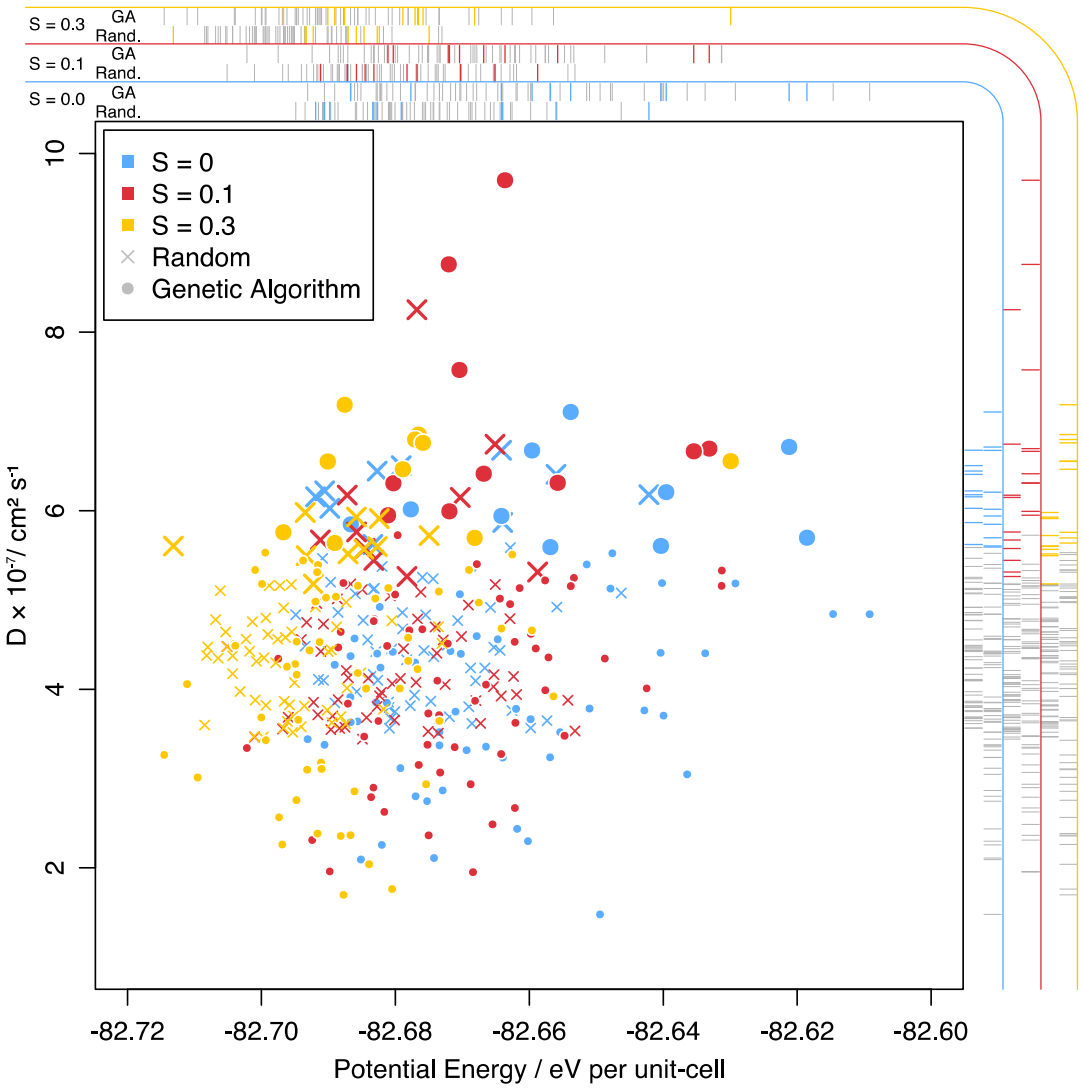

Figure 1 Plot showing the correspondence of Li diffusivity (D) and potential energy for each configuration in random and GA optimised populations. Within each population, the ten configurations with the highest diffusivities are highlighted with larger points. Rug plots attached to the top and right hand margins give an impression of the energy and diffusivity distribution within each population. In order to highlight their position within each, the ten configurations with the highest diffusivities are coloured in the rug plots with the remaining points given in grey.

Within this work, a genetic algorithm has been used to obtain structures with high diffusivities. Following a GA run, the ten configurations from each population, with the highest Li diffusivities were used for further analyses. The structural optimisation made by

the GA was based solely on the Li MSD extracted from each structure. That is, the energy of each configuration was not included as part of the GA's merit function. This could present an issue if the structures obtained from the GA had abnormally high lattice energies, as they would be unlikely to form, even at the high temperatures typical of ceramic processing operations. If so this would mean that the information extracted from their study may be of only limited use.

In order to better understand the correspondence between Li diffusivity and the energy of the optimised structures, potential energy (normalised per unit-cell) is plotted against Li diffusivity for each configuration in the GA optimised population inFig. 1. These are plotted for S=0.0, 0.1 and 0.3 as circles. In order to provide a point of reference, for each S value, diffusivity and energies were plotted for an equivalent population of randomly generated structures as crosses inFig. 1. Values were obtained at T=1000K, structures were initially equilibrated in the NPT ensemble for 25ps before undergoing 50ps of NVE dynamics. Energies were averaged over the course of this NVE period and the Li diffusivity values were also measured over this 50ps period.

In order to understand the energy and diffusivity distributions within each population rug plots have been attached to the top and right hand sides of the figure These serve a similar purpose to histograms: each line within the rug plots corresponds to a point in the scatter plot and the density of these lines is easily observed allowing the overall shape and range of the distributions to be judged.

Within the energy distributions at the top of Fig. 1, it can be seen that for both the random and GA populations, the S=0.3 structures tended to have the lowest energies, followed by S=0.1 and S=0.0 whose distributions appear translated along the energy axis to higher values. Comparing the random and GA optimised distributions, the GA energies span wider range. Interestingly, in the case of the S=0.1 and 0.0, the modal values for these distributions are very similar to their respective random populations (indicating that the increased energies only affect a relatively small number of GA population members). The effect of the GA on the S=0.1 population was to widen and shift the distribution to higher energies, when compared to the random distribution. In order to highlight the correspondence between high diffusivity and system energy, the bars for the configurations with the top ten highest

diffusivities have been highlighted in colour for the GA and random populations respectively (the other bars are given in grey).

It should be noted that the majority of the top ten diffusivities lie within the higher energy region of the energy rug-plots, showing that the best GA optimised structures show a slight bias to higher energies. Notwithstanding this, it should be noted that the difference in energy between the highest and lowest energies, across all structures, was only on the order of 0.1 eV. Furthermore, for S=0.0 six of the top ten points lie within the energy bounds of its respective random distribution. Similarly, eight of the ten points intersect the random distribution energy ranges for S=0.1 and 0.3. In general, it can be concluded that the structures obtained using the GA technique have comparable energies to those chosen from a random distribution (it should be noted that other computational studies employ randomly selected configurations). In addition, the narrow range of energies observed is consistent with the range of thermal energies experienced during high temperature ceramic processing. It therefore seems plausible that structures, with energies on the order of those obtained using the GA, may be kinetically stabilised on cooling from the high temperatures typically used during ceramic manufacture and would therefore be expressed in LLTO materials, even at room temperature. The study of the GA generated structures should therefore provide genuine insight into the mechanisms and properties of these materials.

References

17. S. Stramare, V. Thangadurai and W. Weppner, *Chem. Mater.*, 2003, **15**, 3974.

20. J. Ibarra, A. Várez, C. León, J. Santamara, L. M. Torres-Martinez and J. Sanz, *Solid State Ionics*, 2000, **134**, 219.
21. O. Bohnke, C. Bohnke and J. L. Fourquet, *Solid State Ionics*, 1996, **91**, 21.
22. J. L. Fourquet, H. Duroy and M. P. Crosnier-Lopez, *J. Solid State Chem.*, 1996, **127**, 283.
23. F. Vink and H. Kröger, *Solid State Phys.*, 1956, **3**, 307.
24. K. Ohara, Y. Kawakita, L. Pusztai, L. Temleitner, S. Kohara, N. Inoue and S. Takeda, *J. Phys. Condens.: Matter.*, 2010, **22**, 404203.
27. R. L. Johnston, *Dalt. Trans.*, 2003, 4193.
30. A. Cleave, Ph.D. thesis, Imperial College London (2006).
39. R. A. Buckingham, *Proc. R. Soc. Lond. A.*, 1938, **168**, 264.
41. X. Gao, C. A. J. Fisher, T. Kimura, Y. H. Ikuhara, H. Moriwake, A. Kuwabara, H. Oki, T. Tojigamori, R. Huang Y. Ikuhara, *J. Am. Chem. Soc.*, 2012, **25**, 1607.
42. W. Smith and T. R. Forester, *J. Mol. Graph.*, 1996, **14**, 136.
43. M. Born and J. Mayer, *Z. Phys.*, 1932, **75**, 1.
44. P. Ewald, *Ann. Phys.*, 1921, **369**, 253.

45. S. Nosé, *J. Chem. Phys*., 1984, **81**, 511.
46. S. Nosé, *Mol. Phys.*, 1984, **52**, 255.
47. W. Hoover, *Phys. Rev. A.*, 1985, **31**, 1695.